Journal of Computational Physics 518 (2024) 113340

Contents lists available at ScienceDirect

Journal of Computational Physics

journal homepage: www.elsevier.com/locate/jcp

A second-order, mass-conservative, unconditionally stable and bound-preserving finite element method for the quasi-incompressible Cahn-Hilliard-Darcy system

Yali Gao [a], Daozhi Han [b,*], Xiaoming Wang [c,d]

[a] School of Mathematics and Statistics, Northwestern Polytechnical University, Xi'an, China
[b] Department of Mathematics, State University of New York at Buffalo, Buffalo, NY 14260, United States of America
[c] Department of Mathematics and Statistic, Missouri University of Science and Technology, Rolla, MO 65409, United States of America
[d] School of Mathematical Science, Eastern Institute of Technology, Ningbo, Zhejiang 315200, China

ARTICLE INFO

MSC:
35K61
76T99
76S05
76D07

Keywords:
Cahn-Hilliard-Darcy
Quasi-incompressible
Variable density
Bound-preserving
Second order accuracy
Energy stability

ABSTRACT

A second-order numerical method is developed for solving the quasi-incompressible Cahn-Hilliard-Darcy system with the Flory-Huggins potential for two immiscible fluids of variable densities and viscosities in a porous medium or a Hele-Shaw cell. We show that the scheme is uniquely solvable, mass-conservative, bound-preserving and unconditionally energy stable. The key for bound-preserving is the utilization of second order convex-concave splitting of the logarithmic potential, and the discrete L^1 estimate of the singular potential. Ample numerical tests are reported to validate the accuracy and robustness of the proposed numerical scheme.

1. Introduction

Two immiscible fluids of different characteristics (density, viscosity, mobility etc) in a porous medium or a Hele-Shaw cell are of practical importance in oil recovery [17,53], alloy solidification [69], tumour growth [64] and various other fields [8,26,42,48]. The interface separating different fluids tends to be unstable, which is associated with phenomena such as wave-breaking or tip-splitting [40]. The instability arises if the heavier fluid is above the lighter one (Rayleigh-Taylor instability) or when the less viscous fluid is displacing the more viscous one. The latter, known as Saffman-Taylor instability [53], is unique for two-phase flow in porous media or Hele-Shaw cells. As a consequence the sharp interface formulation-the Muskat problem [51]- could be mathematically ill-posed and singularity could develop in finite time, cf. [22,30] for recent survey in this regard. One possible relaxation without surface tension effect is proposed in [52] utilizing the idea of gradient flows. A different modeling approach is the phase field models where the sharp interface is replaced by a diffusive layer of finite width. Systematic derivation of diffuse interface models for two-phase flows in a porous medium could be based on variational principles [26,36], or from upscaling the Cahn-Hilliard-(Navier)-Stokes equations [23,54,55,11,4]. Derivation of the Cahn-Hilliard-Hele-Shaw system in a Hele-Shaw cell is reported in [44,10,12].

* Corresponding author.
E-mail addresses: gaoylimath@nwpu.edu.cn (Y. Gao), daozhiha@ub.edu (D. Han), xiaomingwang@mst.edu (X. Wang).

https://doi.org/10.1016/j.jcp.2024.113340
Received 30 March 2024; Received in revised form 25 July 2024; Accepted 3 August 2024

Available online 7 August 2024

In this contribution we focus on solving a quasi-incompressible Cahn-Hilliard-Darcy system with the Flory-Huggins potential (qCHD) for two immiscible fluids of different density and viscosity in a porous medium or a Hele-Shaw cell. The model, Eqs. (2.1)–(2.5), can be readily derived by Onsager's extremum principle following [36], employing mass-averaged mixture velocity [47] and using volume fraction difference as the order parameter. We refer to [29,32,61] for numerical methods for solving the quasi-incompressible Cahn-Hilliard-Navier-Stokes system.

A particular challenge in solving phase field fluid models is the stiffness from the diffusive interface (sharp transition in thin layers). Unconditionally stable time marching schemes are preferred so that stiffness can be resolved adaptively without a severe time-step constraint. Several successful strategies emerge in recent years, including the convex-concave splitting [15,16,56,25], the stabilized linear approach [59], the Invariant Energy Quadratization (Lagrange multiplier) method [31,65,66,27], and the Scalar Auxiliary Variable approach [57,58]. Applications of these methods to phase field fluid models can be found in [43,39,18,37,60,35, 13,70,33,28,20].

In phase field fluid models the order parameter represents phase concentration and is necessary to stay bounded between 0 and 1 so that density and viscosity of the mixture can be meaningfully defined. This bound is enforced through nonlinear mechanisms such as degenerate mobility or logarithmic potential in the fourth order Cahn-Hilliard equation. Numerically preserving these nonlinear estimates prove delicate and difficult in practice. To date there are only a few low-order accurate bound-preserving numerical methods for phase field fluid models which are inadequate in capturing rich interfacial dynamics. Early attempts focus on first-order methods, including methods preserving the entropy estimate from the degenerate mobility [71] or schemes maintaining the L^2 estimate of the derivative of the logarithmic potential [9]. Brute-force cut-off of the order parameter often leads to loss of conservation, and as a result it is difficult to obtain high-order accuracy. Instead of direct cut-off one may impose point-wise bounds through either variational inequality [1] or Lagrange multipliers [7]. Another viable approach of cut-off is to perform post-processing by high-order limiters [68,19,45]. A notable high-order limiter is recently constructed in [46] for solving the Cahn-Hilliard-Navier-Stokes equations. However, schemes with post-processing in general do not satisfy the energy law. In [41] a different strategy is proposed in which the bounds are preserved through a change of variable at the expense of possible loss of consistency. Recent development in the design of bound-preserving schemes include the JKO method for optimal transport [21], the exponential differencing method [14], and methods based on convex-concave splitting [5].

In this article we design a second-order finite element method for the qCHD system with variable densities and viscosities. The nonlinear scheme is shown to maintain all favorable properties: unique solvability, unconditional stability, discrete mass-conservation and bound-preserving. The key in the design is second-order convex-splitting (Crank-Nicolson approximation with Admas-Bashforth extrapolation) for the logarithmic potential, see also [37]. This discretization alone seemingly leads to a loss of the L^2 estimate of the singular potential. To make up for the loss and gain bound-preservation, the convex part of the singular potential is brought back as a temporal perturbation to the equation [6]. This strategy allows for a discrete L^1 estimate of the singular potential, thereby preserving the desired bounds for the order parameter. To the best of our knowledge, this is the first second order bound-preserving scheme for a quasi-incompressible phase field model. The method can be readily applied for solving the Cahn-Hilliard-Navier-Stokes equations of matched densities (Model H), and could be potentially generalized for higher order accuracy. However the scheme is not applicable to the quasi-incompressible Cahn-Hilliard-Navier-Stokes system, since the well-posedness of the model with the logarithmic potential remains open.

The outline of this paper is as follows. In Section 2, we present the quasi-incompressible Cahn-Hilliard-Darcy equations and its weak formulation. In Section 3, we present the numerical scheme and establish its unique solvability, energy stability, mass-conservation and bound-preserving. In Section 4, numerical results are reported to verify the accuracy and efficiency of the numerical method.

2. The quasi-incompressible Cahn-Hilliard-Darcy system

We consider the following quasi-incompressible Cahn-Hilliard-Darcy equations (qCHD) for two-phase flows in a porous region $\Omega \subset \mathbb{R}^3$:

$$\Pi^{-1}\eta(\phi)\boldsymbol{u} = -\nabla p - \frac{1}{\epsilon Ca^*}\phi\nabla\mu - \frac{Bo}{Ca^*}\rho\boldsymbol{k}, \tag{2.1}$$

$$\nabla\cdot\boldsymbol{u} = \frac{\alpha}{Pe}\Delta\mu_p, \tag{2.2}$$

$$\partial_t(\chi\phi) + \nabla\cdot(\phi\boldsymbol{u}) = \frac{1}{Pe}\Delta\mu_p, \tag{2.3}$$

$$\mu = f(\phi) - \epsilon^2\Delta\phi, \tag{2.4}$$

$$\mu_p = \mu + \alpha\epsilon Ca^* p, \tag{2.5}$$

equipped with the boundary conditions

$$\boldsymbol{u}\cdot\boldsymbol{n} = \nabla\phi\cdot\boldsymbol{n} = \nabla\mu_p\cdot\boldsymbol{n} = 0, \quad \text{on } \Gamma := \partial\Omega.$$

Here Π is the permeability, the non-dimensionalized density and viscosity of the binary fluid are

$$\rho = \frac{1-\phi}{2} + \frac{1+\phi}{2}\frac{\rho_2}{\rho_1}, \quad \eta(\phi) = \frac{1-\phi}{2} + \frac{1+\phi}{2}\frac{\eta_2}{\eta_1},$$

where $\rho_1, \rho_2; \eta_1, \eta_2$ are the densities and viscosities of the two fluids, respectively. ϵ is the Cahn number (a measure of relative thickness of the diffusive interface), Ca^* is the modified capillary number, $\boldsymbol{k}$ is the unit vector in the vertical direction, Bo is the Bond number, χ is the porosity, Pe is the Peclet number, $\alpha = \frac{\rho_1 - \rho_2}{\rho_1 + \rho_2}$ is a constant. Here $f = F'$, and $F(\phi)$ is the logarithmic Flory-Huggins free energy density function

$$F(\phi) = \frac{\theta}{2}[(1+\phi)\ln(1+\phi) + (1-\phi)\ln(1-\phi)] - \frac{\theta_c}{2}\phi^2, \tag{2.6}$$

with θ the absolute temperature of the mixture, and θ_c the critical temperature, $0 < \theta < \theta_c$. In the case θ is close to θ_c, F is often approximated by a polynomial of double-well type. On the other hand, when θ approaches zero, one obtains the double obstacle potential. The qCHD system can be derived via Onsager's extremum principle, cf. [36].

The definition of ρ and the Eq. (2.3) imply the continuity equation

$$\partial_t(\chi\rho) + \nabla\cdot(\rho\boldsymbol{u}) = 0. \tag{2.7}$$

Introducing the total energy of the system

$$E(\phi) := \frac{1}{Ca^*}\int_\Omega \frac{1}{\epsilon}F(\phi) + \frac{\epsilon}{2}|\nabla\phi|^2 + Bo\rho z\, d(\chi\boldsymbol{x}), \tag{2.8}$$

one deduces that the qCHD system (2.1)-(2.4) satisfies an energy dissipation law

$$\frac{d}{dt}E = -\frac{1}{Pe\epsilon Ca^*}\int_\Omega |\nabla\mu_p|^2\, d\boldsymbol{x} - \int_\Omega \Pi^{-1}\eta|\boldsymbol{u}|^2\, d\boldsymbol{x}. \tag{2.9}$$

Let $Q_{s,t}$ denote $\Omega\times(s,t)$ and $Q = Q_{0,T}$ for fixed $T > 0$. The L^2 inner product and norm are denoted by $(\cdot,\cdot)$ and $||\cdot||$, respectively. We introduce $M := H^1(\Omega)\cap L_0^2(\Omega)$ with $L_0^2(\Omega)$ the subspace of $L^2(\Omega)$ of mean zero; $\mathbf{X} := [L^2(\Omega)]^3$, $Y := H^1(\Omega)$, Y' the dual of Y, and $\langle\cdot,\cdot\rangle$ the duality between Y' and Y. The weak formulation of the qCHD system is defined as follows.

Definition 2.1. Assume $\phi_0 \in L^\infty(\Omega)\cap Y$ with $-1 < \phi_0 < 1$ a.e.. Then $\left(\rho, \phi, \boldsymbol{u}, \mu_p, p\right)$ is called a weak solution of the system (2.1)-(2.4) on time interval $[0,T]$ if

$$\phi \in L^\infty(0,T;Y)\cap H^1(0,T;Y')\cap L^4(0,T;H^2(\Omega)),$$
$$f(\phi)\in L^2(Q),\quad \phi\in L^\infty(Q),\quad |\phi|<1\quad a.e.,$$
$$\boldsymbol{u}\in L^2(0,T;\mathbf{X}),\quad p\in L^2(0,T;M),$$
$$\mu_p\in L^2(0,T;Y),$$

and, for $t\in(0,T)$ a.e.

$$\langle\partial_t(\chi\phi),\varphi\rangle - (\phi\boldsymbol{u},\nabla\varphi) = -\frac{1}{Pe}(\nabla\mu_p,\nabla\varphi),\forall\varphi\in Y, \tag{2.10}$$
$$(\mu,\varphi) = (f(\phi),\varphi) + \epsilon^2(\nabla\phi,\nabla\varphi),\forall\varphi\in Y, \tag{2.11}$$
$$(\Pi^{-1}\eta(\phi)\boldsymbol{u},\boldsymbol{v}) = -(\nabla p,\boldsymbol{v}) - \frac{1}{\epsilon Ca^*}(\phi\nabla\mu,\boldsymbol{v}) - \frac{Bo}{Ca^*}(\rho\boldsymbol{k},\boldsymbol{v}),\forall\boldsymbol{v}\in\mathbf{X}, \tag{2.12}$$
$$(\boldsymbol{u},\nabla\varphi) = \frac{\alpha}{Pe}(\nabla\mu_p,\nabla\varphi),\forall\varphi\in Y, \tag{2.13}$$

where for $(\boldsymbol{x},t)\in Q$ a.e.

$$\mu_p = \mu + \alpha\epsilon Ca^* p,\quad \rho = \frac{1-\phi}{2} + \frac{1+\phi}{2}\frac{\rho_2}{\rho_1}. \tag{2.14}$$

3. The second order numerical scheme

Since the parameters do not affect the properties of the scheme, we set them to be unity except α in the following presentation.

Let $\mathcal{T}_h$ be a quasi-uniform triangulation of Ω. Let $Y_h \subset Y$ be the finite element space of continuous piecewise linear functions on $\overline{\Omega}$. The collection of nodes on $\mathcal{T}_h$ is $\{\boldsymbol{x}_i\}_{i=1}^{N_h}$, while the set of nodal basis functions is denoted by $\{\chi_i\}_{i=1}^{N_h}$. The interpolation operator $I_h : C(\overline{\Omega})\to Y_h$ is defined such that $I_h(\phi)(\boldsymbol{x}_i) = \phi(\boldsymbol{x}_i), i = 1,\dots N_h$. One introduces the discrete inner product

$$(\phi,\varphi)_h := \int_\Omega I_h(\phi\varphi)\, d\boldsymbol{x} = \sum_{i=1}^{N_h} w_i\phi(\boldsymbol{x}_i)\varphi(\boldsymbol{x}_i)$$

with $w_i = \int_\Omega \chi_i\, d\boldsymbol{x}$. The associated semi-norm is denoted by $||\cdot||_h$, which is equivalent to the L^2 norm on Y_h. Let $M_h := Y_h\cap L_0^2(\Omega)$. One also introduces the discrete L^1 norm

$$||\phi_h||_{1,h} := (|\phi_h|, 1)_h = \sum_{i=1}^{N_h} w_i |\phi_h(\boldsymbol{x}_i)|.$$

Let $0 = t_0 < t_1 < \cdots < t_M = T$ be a uniform partition of $[0, T]$ into sub-intervals $J^n = (t_n, t_{n+1})$, $n = 0, 1, \ldots, M-1$, with time step size $\Delta t = t_{n+1} - t_n = \frac{T}{M}$. Throughout, we adopt the following notations

$$\delta_t \phi^{n+1} := \frac{\phi^{n+1} - \phi^n}{\Delta t}, \quad \phi^{n+\frac{1}{2}} = \frac{1}{2}(\phi^{n+1} + \phi^n), \quad \tilde{\phi}^{n+\frac{1}{2}} = \frac{3\phi^n - \phi^{n-1}}{2}.$$

The fully discrete finite element scheme for the qCHD equations reads: given $\phi_h^{n-1}, \phi_h^n \in Y_h$ with $|\phi_h^{n-1}(\boldsymbol{x}_i)| < 1$ and $|\phi_h^n(\boldsymbol{x}_i)| < 1$ for $i = 1 \cdots N_h$, find $(\phi_h^{n+1}, \mu_h^{n+\frac{1}{2}}, \boldsymbol{u}_h^{n+\frac{1}{2}}, p_h^{n+\frac{1}{2}}) \in Y_h \times Y_h \times \mathbf{X_h} \times M_h$ such that

$$\left(\delta_t(\phi_h^{n+1}), \varphi\right)_h - ([\tilde{\phi}_h^{n+\frac{1}{2}}]\boldsymbol{u}_h^{n+\frac{1}{2}}, \nabla\varphi) = -(\nabla \mu_{p,h}^{n+\frac{1}{2}}, \nabla\varphi), \quad \forall \varphi \in Y_h, \tag{3.1}$$

$$(\mu_h^{n+\frac{1}{2}}, \varphi)_h = \left(\frac{F_v(\phi_h^{n+1}) - F_v(\phi_h^n)}{\phi_h^{n+1} - \phi_h^n}, \varphi\right)_h + \left(f_n(\tilde{\phi}_h^{n+\frac{1}{2}}), \varphi\right) + (\nabla \phi_h^{n+\frac{1}{2}}, \nabla\varphi)$$
$$+ \Delta t \left(f_v(\phi_h^{n+1}) - f_v(\phi_h^n), \varphi\right)_h, \quad \forall \varphi \in Y_h, \tag{3.2}$$

$$(\eta([\tilde{\phi}_h^{n+\frac{1}{2}}])\boldsymbol{u}_h^{n+\frac{1}{2}}, \boldsymbol{v}) = -(\nabla p_h^{n+\frac{1}{2}}, \boldsymbol{v}) - ([\tilde{\phi}_h^{n+\frac{1}{2}}]\nabla \mu_h^{n+\frac{1}{2}}, \boldsymbol{v}) - \left(\rho([\tilde{\phi}_h^{n+\frac{1}{2}}])\boldsymbol{k}, \boldsymbol{v}\right), \quad \forall \boldsymbol{v} \in \mathbf{X}_h, \tag{3.3}$$

$$(\boldsymbol{u}_h^{n+\frac{1}{2}}, \varphi) = \alpha(\nabla \mu_{p,h}^{n+\frac{1}{2}}, \nabla\varphi), \quad \forall \varphi \in Y_h, \tag{3.4}$$

where $f_v = F_v', f_n = F_n'$ correspond to convex-concave splitting of F, i.e.

$$f_v(\phi) = \frac{\theta}{2}\left[\ln(1+\phi) - \ln(1-\phi)\right], \quad f_n(\phi) = -\theta_c \phi. \tag{3.5}$$

Here $[x]$ represents a truncation of x such that

$$[x] = \begin{cases} 1, & x \geq 1, \\ x, & x \in (-1, 1), \\ -1, & x \leq -1. \end{cases}$$

In the scheme (3.1)–(3.4) the Darcy equations are solved in a mixed form. We notice that the velocity can be found explicitly from Eq. (3.3). One can also construct a scheme by eliminating the velocity variable: given $\phi_h^{n-1}(\boldsymbol{x}_i), \phi_h^n(\boldsymbol{x}_i) \in Y_h$ with $|\phi_h^{n-1}| < 1$ and $|\phi_h^n| < 1$ for $i = 1 \cdots N_h$, find $(\phi_h^{n+1}, \mu_h^{n+\frac{1}{2}}, p_h^{n+\frac{1}{2}}) \in Y_h \times Y_h \times M_h$ such that

$$\left(\delta_t \phi_h^{n+1}, \varphi\right)_h - ([\tilde{\phi}_h^{n+\frac{1}{2}}]\boldsymbol{u}_h^{n+\frac{1}{2}}, \nabla\varphi) = -(\nabla \mu_{p,h}^{n+\frac{1}{2}}, \nabla\varphi), \quad \forall \varphi \in Y_h, \tag{3.6}$$

$$(\mu_h^{n+\frac{1}{2}}, \varphi)_h = \left(\frac{F_v(\phi_h^{n+1}) - F_v(\phi_h^n)}{\phi_h^{n+1} - \phi_h^n}, \varphi\right)_h + \left(f_n(\tilde{\phi}_h^{n+\frac{1}{2}}), \varphi\right) + (\nabla \phi_h^{n+\frac{1}{2}}, \nabla\varphi)$$
$$+ \Delta t \left(f_v(\phi_h^{n+1}) - f_v(\phi_h^n), \varphi\right)_h, \quad \forall \varphi \in Y_h, \tag{3.7}$$

$$(\boldsymbol{u}_h^{n+\frac{1}{2}}, \varphi) = \alpha(\nabla \mu_{p,h}^{n+\frac{1}{2}}, \nabla\varphi), \quad \forall \varphi \in Y_h, \tag{3.8}$$

where

$$\eta([\tilde{\phi}_h^{n+\frac{1}{2}}])\boldsymbol{u}_h^{n+\frac{1}{2}} := -\nabla p_h^{n+\frac{1}{2}} - [\tilde{\phi}_h^{n+\frac{1}{2}}]\nabla \mu_h^{n+\frac{1}{2}} - \rho([\tilde{\phi}_h^{n+\frac{1}{2}}])\boldsymbol{k}, \tag{3.9}$$

$$\mu_{p,h}^{n+\frac{1}{2}} = \mu_h^{n+\frac{1}{2}} + \alpha p_h^{n+\frac{1}{2}}, \tag{3.10}$$

$$\rho([\tilde{\phi}_h^{n+\frac{1}{2}}]) = \frac{1}{2}(1 - [\tilde{\phi}_h^{n+\frac{1}{2}}]) + \frac{1}{2}(1 + [\tilde{\phi}_h^{n+\frac{1}{2}}])\frac{\rho_2}{\rho_1}. \tag{3.11}$$

Note that $\tilde{\phi}_h^{n+\frac{1}{2}}$ may be outside of $(-1, 1)$ although both ϕ_h^n and ϕ_h^{n-1} provably satisfy the bounds at the nodes of $\mathcal{T}_h$. The truncation of $\tilde{\phi}_h^{n+\frac{1}{2}}$ appears necessary in the estimate of pressure in terms of the generalized chemical potential μ_p. Indeed, recalling $\alpha = \frac{\rho_1 - \rho_2}{\rho_1 + \rho_2}$ and noting Eq. (3.11), one can rewrite the Darcy equations (3.9) as

$$\eta([\tilde{\phi}_h^{n+\frac{1}{2}}])\boldsymbol{u}_h^{n+\frac{1}{2}} = -\frac{2\rho_1}{\rho_1 + \rho_2}\rho([\tilde{\phi}_h^{n+\frac{1}{2}}])\nabla p_h^{n+\frac{1}{2}} - [\tilde{\phi}_h^{n+\frac{1}{2}}]\nabla \mu_{p,h}^{n+\frac{1}{2}} - \rho([\tilde{\phi}_h^{n+\frac{1}{2}}])\boldsymbol{k}. \tag{3.12}$$

It is clear that the truncation is needed so that $\rho([\tilde{\phi}_h^{n+\frac{1}{2}}])$ has a positive lower bound, cf. Step 3 in the proof of the main theorem below.

Combining Eq. (3.6) and Eq. (3.8) one obtains

$$\alpha\left(\delta_t\phi_h^{n+1},\varphi\right)_h+\left((1-\alpha[\tilde{\phi}_h^{n+\frac{1}{2}}])\boldsymbol{u}_h^{n+\frac{1}{2}},\nabla\varphi\right)=0.$$

In light of definition of ρ in (2.14) one verifies that the scheme satisfies the continuity equation

$$\left(\delta_t\rho(\phi_h^{n+1}),\varphi\right)_h-\left(\rho([\tilde{\phi}_h^{n+\frac{1}{2}}])\boldsymbol{u}_h^{n+\frac{1}{2}},\nabla\varphi\right)=0. \tag{3.13}$$

The schemes are three-level methods. To initiate, one could carry out one iterate of a first-order version of the current scheme:

$$\left(\delta_t\phi_h^1,\varphi\right)_h-(\phi_h^0\boldsymbol{u}_h^1,\nabla\varphi)=-(\nabla\mu_{p,h}^1,\nabla\varphi),\quad\forall\varphi\in Y_h, \tag{3.14}$$

$$(\mu_h^1,\varphi)_h=\left(f_v(\phi_h^1),\varphi\right)_h+\left(f_n(\phi_h^0),\varphi\right)+(\nabla\phi_h^1,\nabla\varphi),\quad\forall\varphi\in Y_h, \tag{3.15}$$

$$(\boldsymbol{u}_h^1,\nabla\varphi)=\alpha(\nabla\mu_{p,h}^1,\nabla\varphi),\quad\forall\varphi\in Y_h, \tag{3.16}$$

with

$$\eta(\phi_h^0)\boldsymbol{u}_h^1:=-\nabla p_h^1-\phi_h^0\nabla\mu_h^1-\rho(\phi_h^0)\boldsymbol{k},$$
$$\mu_{p,h}^1=\mu_h^1+\alpha p_h^1,$$
$$\rho(\phi_h^0)=\frac{1}{2}(1-\phi_h^0)+\frac{1}{2}(1+\phi_h^0)\frac{\rho_2}{\rho_1}.$$

It will be clear from the monotone argument below that (3.14)–(3.16) is uniquely solvable. In particular, under the assumption $\phi_h^0\in Y_h$ such that $|\phi_h^0|\le 1$ and $\overline{\phi_h^0}:=\frac{1}{|\Omega|}\int_\Omega\phi_h^0\,d\boldsymbol{x}\in(-1,1)$, there exists $\delta_1>0$ such that

$$|\phi_h^1(\boldsymbol{x}_i)|\le 1-\delta_1,\quad i=1\dots N_h. \tag{3.17}$$

Indeed this follows from the L^1 estimate by taking $\varphi=\phi_h^1-\overline{\phi_h^0}$ in Eq. (3.15), cf. the estimates (3.21)–(3.25).

The following elementary inequality is useful, see also [49, Proposition 4.3].

Lemma 3.1. *Suppose $|\phi_h^n(\boldsymbol{x}_i)|\le 1-\delta, i=1\dots N_h$ for sufficiently small $\delta>0$. Then there exist constants $C_1,C_2>0$ independent of δ such that*

$$f_v(s)(s-\phi_h^n(\boldsymbol{x}_i))\ge C_1\delta|f_v(s)|-C_2,\quad\forall s\in(-1,1),\quad i=1\dots N_h. \tag{3.18}$$

Proof. Define

$$g(s)=f_v(s)(s-\phi_h^n(\boldsymbol{x}_i))-\frac{\delta}{2}f_v(s)s=f_v(s)\left[(1-\frac{\delta}{2})s-\phi_h^n(\boldsymbol{x}_i)\right].$$

Thanks to $|\phi_h^n(\boldsymbol{x}_i)|\le 1-\delta$, one verifies that

$$g\to+\infty,\quad s\to\pm1.$$

Since g is smooth in $(-1,1)$, there exists $C\ge 0$ such that $g\ge -C$. The inequality (3.18) then follows from the fact [49, (4.6)]

$$f_v(s)s\ge C_3|f_v(s)|-C_4.$$

This completes the proof. □

Remark 3.1. If $\phi_h^n(\boldsymbol{x}_i)$ in (3.18) is replaced by a constant between -1 and 1, then there would be no δ in the inequality (3.18).

The unique solvability, energy stability and bound-preserving properties of the scheme are summarized in the following theorem.

Theorem 3.1. *Assume $\phi_h^0\in Y_h$ such that $E(\phi_h^0)<\infty$, $|\phi_h^0|\le 1$ and $\frac{1}{|\Omega|}\int_\Omega\phi_h^0\,d\boldsymbol{x}\in(-1,1)$, and the scheme is initialized by (3.14)–(3.16). Then for any $h,\Delta t>0$ the scheme (3.6)–(3.11) admits a unique solution such that*

$$|\phi_h^n(\boldsymbol{x}_i)|<1,\quad n=1,2\dots M, i=1\dots N_h.$$

Furthermore the scheme is mass-conservative in the sense of satisfying the continuity equation (3.13). Finally the following discrete energy law holds: for any $1\le m\le M-1$

$$\int_\Omega I_h F_v(\phi_h^{m+1}) + F_n(\phi_h^{m+1}) + \frac{1}{2}||\nabla\phi_h^{m+1}||^2 + \rho(\phi_h^{m+1})z\,d\boldsymbol{x} + \frac{1}{4}||\phi_h^{m+1} - \phi_h^m||^2$$
$$+ \Delta t \sum_{n=1}^{m} \int_\Omega \eta([\tilde{\phi}_h^{n+\frac{1}{2}}])|\boldsymbol{u}_h^{n+\frac{1}{2}}|^2 + |\nabla\mu^{n+\frac{1}{2}}|^2\,d\boldsymbol{x}$$
$$\le \int_\Omega I_h F_v(\phi_h^1) + F_n(\phi_h^1) + \frac{1}{2}||\nabla\phi_h^1||^2 + \rho(\phi_h^1)z\,d\boldsymbol{x} + \frac{1}{4}||\phi_h^1 - \phi_h^0||^2. \tag{3.19}$$

Proof. We follow the monotone argument from [37] to show the unique existence of solution to Eqs. (3.6)–(3.11). We divide the proof into several steps. We temporarily drop the dependence on h and n for the solutions.

Step 1. Claim: for a given $\mu \in Y_h$, Eqs. (3.8)–(3.11) admit a unique solution $p \in M_h$, and the solution p depends continuously on μ in the H^1 norm.

The Eq. (3.8) and (3.9) is a linear system of finite dimension. The solvability is a consequence of uniqueness which is in turn a byproduct of continuous dependence. The continuous dependency is easily seen since the equations amount to a Poisson problem for pressure

$$-\left(\eta^{-1}([\tilde{\phi}_h^{n+\frac{1}{2}}])\left(\nabla p - \tilde{\phi}_h^{n+\frac{1}{2}}\nabla\mu - \rho([\tilde{\phi}_h^{n+\frac{1}{2}}])\mathbf{k}\right), \nabla\varphi\right) = \alpha(\nabla\mu + \alpha\nabla p, \nabla\varphi).$$

It then follows from Eq. (3.9) that $\boldsymbol{u}$ in the L^2 norm continuously depends on μ in the H^1 norm.

Step 2. Claim: for a given $\mu \in Y_h$, there is a unique solution $\phi \in Y_h$ to the Eq. (3.7) such that $|\phi(\boldsymbol{x}_i)| < 1 - \delta_\mu, i = 1 \cdots N_h$ for a small positive constant δ_u that depends on μ.

There are two methods of proving the claim: one classical way is to truncate the singular potential f_v and proceed with compactness argument [9,49]; the other method is to argue by contradiction in the same spirit of strong maximum principle [6,67]. Here we outline the first approach but omit some details since they can be found in the references.

For a large $N > 0$, one introduces a truncation of f_v as follows [49, pp 63]:

$$f_v^N(s) = \begin{cases} f_v(-1+N^{-1}) + f_v'(-1+N^{-1})(s+1-N^{-1}), & s < -1+N^{-1}, \\ f_v(s), \quad |s| \le 1-N^{-1}, \\ f_v(1-N^{-1}) + f_v'(1-N^{-1})(s-1+N^{-1}), & s > 1-N^{-1}, \end{cases}$$

and the associated convex potential is defined as $F_v^N := \int_0^s f_v^N(x)\,dx$. One notes that for sufficiently large N f_v^N satisfies the inequality (3.18) as well, cf. [49, (4.12)].

One then considers the approximate system

$$(\mu,\varphi)_h = \left(G^N(\phi^N),\varphi\right)_h + \left(f_n(\tilde{\phi}_h^{n+\frac{1}{2}}),\varphi\right) + \frac{1}{2}(\nabla\phi^N,\nabla\varphi) + \frac{1}{2}(\nabla\phi_h^n,\nabla\varphi)$$
$$+ \Delta t\left(f_v^N(\phi^N) - f_v(\phi_h^n),\varphi\right)_h, \quad \forall\varphi \in Y_h, \tag{3.20}$$

where $G^N(\phi^N) := \frac{F_v^N(\phi^N) - F_v^N(\phi_h^n)}{\phi^N - \phi_h^n}$ is monotonically increasing for fixed ϕ_h^n thanks to the convexity of F_v^N. For a given $\mu \in Y_h$, Eq. (3.20) is uniquely solvable since it is the Euler-Lagrange equation of the following strictly convex functional

$$J(\phi) := \left(\int_0^\phi G^N(s)\,ds, 1\right)_h + \Delta t\left(F_v^N(\phi), 1\right)_h + \int_\Omega \frac{1}{4}|\nabla\phi|^2\,d\boldsymbol{x}$$
$$- \left(\mu + \Delta t f_v(\phi_h^n), \phi\right)_h + \left(f_n(\tilde{\phi}_h^{n+\frac{1}{2}}) - \frac{1}{2}\Delta_h\langle\phi_h^n\rangle, \varphi\right),$$

on the admissible set of finite dimension

$$A_h := \left\{\phi \in Y_h, \int_\Omega \phi\,d\boldsymbol{x} = \int_\Omega \phi_h^n\,d\boldsymbol{x}\right\}.$$

Here the discrete Laplacian operator $-\Delta_h : M_h \to M_h$ is such that

$$(-\Delta_h\phi,\varphi) = (\nabla\phi,\nabla\varphi), \quad \forall\varphi \in Y_h,$$

and $\langle\phi\rangle := \phi - \frac{1}{|\Omega|}\int_\Omega \phi\,d\boldsymbol{x}$.

We derive some a priori estimates on ϕ^N that allows passing to the limit. Taking $\varphi = \phi^N - \phi_h^n$ in Eq. (3.20), and noting by the inequality (3.18)

$$\begin{aligned}\left(f_v^N(\phi^N), \phi^N - \phi_h^n\right)_h &= \sum_{i=1}^{N_h} m_i f_v^N\left(\phi^N(\boldsymbol{x}_i)\right)\left(\phi^N(\boldsymbol{x}_i) - \phi_h^n(\boldsymbol{x}_i)\right) \\ &\geq \sum_{i=1}^{N_h} m_i [C_1\delta_n |f_v^N\left(\phi^N(\boldsymbol{x}_i)\right)| - C_2] \\ &= C_1\delta_n ||I_h\left(f_v^N(\phi^N)\right)||_{1,h} - C, \end{aligned} \tag{3.21}$$

one obtains by Poincaré's inequality

$$\begin{aligned}&\left(F_v^N(\phi^N), 1\right)_h + ||\nabla\phi^N||^2 + \delta_n\Delta t||I_h\left(f_v^N(\phi^N)\right)||_{1,h} \leq C||\nabla\mu||^2 + \left(F_v^N(\phi_h^n), 1\right)_h \\ &+ C(||\tilde{\phi}_h^{n+\frac{1}{2}}||^2 + ||\nabla\phi_h^n||^2 + ||I_h\left(f_v(\phi_h^n)\right)||^2). \end{aligned} \tag{3.22}$$

This implies, by Poincaré's inequality, uniform boundedness of $||\phi^N||_h$ and $||\nabla\phi^N||$, independent of N, and hence up to a subsequence

$$\begin{aligned}&\phi^N \to \phi \text{ weakly in } H^1 \text{ and strongly in } L^2, \\ &\phi^N(\boldsymbol{x}_i) \to \phi(\boldsymbol{x}_i), \quad i = 1 \dots N_h. \end{aligned}$$

In light of the fact that all norms are equivalent in finite dimension for fixed h, Eq. (3.22) also implies

$$||I_h\left(f_v^N(\phi^N)\right)||_{L^\infty} \leq C(\Delta t, h, \mu, \delta_n). \tag{3.23}$$

Note that $f_v(s) \to +\infty, s \to 1$. By choosing δ_μ small enough such that $f_v(1-\delta_\mu) > C(\Delta t, h, \mu, \delta_n)$, one obtains for $N > \delta_\mu^{-1}$

$$|f_v^N\left(\phi^N(\boldsymbol{x}_i)\right)| \leq C(\Delta t, h, \mu, \delta_n) < f_v(1-\delta_\mu) = f_v^N(1-\delta_\mu). \tag{3.24}$$

In light of the oddity of f_v, there holds $-f_v^N(1-\delta_\mu) = f_v^N(\delta_\mu - 1)$ for $N > \delta_\mu^{-1}$. The monotonicity of f_v^N then gives $|\phi^N(\boldsymbol{x}_i)| \leq 1-\delta_\mu$, and thereby

$$|\phi(\boldsymbol{x}_i)| \leq 1 - \delta_\mu. \tag{3.25}$$

By the mean value theorem and the uniform boundedness of ϕ^N and ϕ_h^n, one has

$$||G^N(\phi^N)||_h^2 = \sum_{i=1}^{N_h} m_i \left[f_v^N\left(\theta\phi^N(\boldsymbol{x}_i) + (1-\theta)\phi_h^n(\boldsymbol{x}_i)\right)\right]^2 \leq C_\mu.$$

Since $G^N \to G, F_v^N \to F_v, f_v^N \to f_v$ as $N \to \infty$, one can pass to the limit in Eq. (3.20) and conclude that ϕ is the solution to Eq. (3.7).

The continuous dependence of ϕ on μ in H^1 is straightforward in view of the monotonicity of G and f_v. This completes proof of the claim. Note that δ_μ depends on μ at this stage. This dependence will be removed after establishing the energy law in Step 4.

Step 3. Now one introduces an operator $T : Y_h \to Y_h$ such that for a given $\mu \in Y_h$

$$\left(T(\mu), \varphi\right) = (\phi - \phi_h^n, \varphi)_h - \Delta t([\tilde{\phi}_h^{n+\frac{1}{2}}]\boldsymbol{u}, \nabla\varphi) + \Delta t(\nabla\mu_p, \nabla\varphi), \forall\varphi \in Y_h, \tag{3.26}$$

where ϕ is the solution to Eq. (3.7), $\boldsymbol{u}$ and p are solutions to Eqs. (3.8) and (3.9). It is clear from Step 1 and Step 2 that the operator T is continuous and bounded.

Claim: the operator T is strictly monotone in the sense that

$$(T(\mu) - T(\nu), \mu - \nu) \geq 0, \quad \forall\mu, \nu \in Y_h, \tag{3.27}$$

with equality iff $\mu = \nu$.

One has

$$\begin{aligned}&\left(T(\mu) - T(\nu), \mu - \nu\right) = (\phi_\mu - \phi_\nu, \mu - \nu)_h - \Delta t\left([\tilde{\phi}_h^{n+\frac{1}{2}}](\boldsymbol{u}_\mu - \boldsymbol{u}_\nu), \nabla(\mu - \nu)\right) \\ &+ \Delta t\left(\nabla(\mu_p - \nu_p), \nabla(\mu - \nu)\right). \end{aligned} \tag{3.28}$$

Thanks to the monotonicity of G and f_v, Eq. (3.7) implies

$$\begin{aligned}&(\phi_\mu - \phi_\nu, \mu - \nu)_h = \left(G(\phi_\mu) - G(\phi_\nu), \phi_\mu - \phi_\nu\right)_h + \frac{1}{2}||\nabla(\phi_\mu - \phi_\nu)||^2 \\ &+ \Delta t\left(f_v(\phi_\mu) - f_v(\phi_\nu), \phi_\mu - \phi_\nu\right)_h \geq 0, \end{aligned} \tag{3.29}$$

with equality iff $\mu = \nu$. Likewise, one derives from Eqs. (3.8) and (3.9)

$$-\left([\tilde{\phi}_h^{n+\frac{1}{2}}](\boldsymbol{u}_\mu - \boldsymbol{u}_\nu), \nabla(\mu - \nu)\right)$$

$$= \int_\Omega \eta([\tilde{\phi}_h^{n+\frac{1}{2}}])|\boldsymbol{u}_\mu - \boldsymbol{u}_\nu|^2\, d\boldsymbol{x} + \big(\nabla(p_\mu - p_\nu), (\boldsymbol{u}_\mu - \boldsymbol{u}_\nu)\big)$$

$$= \int_\Omega \eta([\tilde{\phi}_h^{n+\frac{1}{2}}])|\boldsymbol{u}_\mu - \boldsymbol{u}_\nu|^2\, d\boldsymbol{x} + \alpha\big(\nabla(\mu_p - \nu_p), \nabla(p_\mu - p_\nu)\big). \tag{3.30}$$

Finally

$$\big(\nabla(\mu_p - \nu_p), \nabla(\mu - \nu)\big) = ||\nabla(\mu_p - \nu_p)||^2 - \alpha\big(\nabla(\mu_p - \nu_p), \nabla(p_\mu - p_\nu)\big). \tag{3.31}$$

Collecting Eqs. (3.29)–(3.31), one concludes

$$\big(T(\mu) - T(\nu), \mu - \nu\big) \geq 0, \quad \forall \mu, \nu \in Y$$

with equality iff $\mu = \nu$. Hence the operator T is strictly monotone.
Claim: the operator T is coercive in the sense that

$$\frac{\big(T(\mu), \mu\big)}{||\mu||_{H^1}} \to \infty, \text{ as } ||\mu||_{H^1} \to \infty. \tag{3.32}$$

One calculates

$$\big(T(\mu), \mu\big) = (\phi - \phi_h^n, \mu)_h - \Delta t([\tilde{\phi}_h^{n+\frac{1}{2}}]\boldsymbol{u}, \nabla\mu) + \Delta t(\nabla\mu_p, \nabla\mu). \tag{3.33}$$

Taking $\varphi = \phi - \phi_h^n$ in Eq. (3.7) and noting the monotonicity of f_v, one deduces by Poincarè's inequality

$$(\phi - \phi^n, \mu)_h \geq \frac{1}{4}||\nabla\phi||^2 + \int_\Omega I^h F_v(\phi)\, d\boldsymbol{x}$$

$$- \Big(C||\nabla\phi_h^n||^2 + \int_\Omega I^h F_v(\phi_h^n)\, d\boldsymbol{x} + C||\tilde{\phi}_h^{n+\frac{1}{2}}||^2\Big). \tag{3.34}$$

Likewise by testing Eqs. (3.9) with $\boldsymbol{u}$ and taking $\varphi = p$ in Eq. (3.8), one obtains

$$-([\tilde{\phi}_h^{n+\frac{1}{2}}]\boldsymbol{u}, \nabla\mu) + (\nabla\mu_p, \nabla\mu) \geq ||\nabla\mu_p||^2 + \frac{1}{2}\int_\Omega \eta([\tilde{\phi}_h^{n+\frac{1}{2}}])|\boldsymbol{u}|^2\, d\boldsymbol{x} - C. \tag{3.35}$$

The pressure gradient is estimated by using the Darcy's equations (3.12)

$$||\nabla p|| \leq C||\sqrt{\eta}\boldsymbol{u}|| + C||\nabla\mu_p|| + C,$$

hence

$$||\nabla\mu|| \leq ||\nabla\mu_p|| + |\alpha|||\nabla p|| \leq C||\sqrt{\eta}\boldsymbol{u}|| + C||\nabla\mu_p|| + C. \tag{3.36}$$

It follows from the estimates (3.34)–(3.36)

$$\big(T(\mu), \mu\big) \geq \Delta t||\nabla\mu_p||^2 + \frac{\Delta t}{2}\int_\Omega \eta([\tilde{\phi}_h^{n+\frac{1}{2}}])|\boldsymbol{u}|^2\, d\boldsymbol{x} + \frac{1}{4}||\nabla\phi||^2 + \int_\Omega I_h F(\phi)\, d\boldsymbol{x} - C$$

$$\geq C||\nabla\mu||^2 + \frac{1}{4}||\nabla\phi||^2 + \int_\Omega I_h F(\phi)\, d\boldsymbol{x} - C. \tag{3.37}$$

Next we estimate $\int_\Omega \mu\, d\boldsymbol{x}$. By the mean value theorem,

$$G\big(\phi(\boldsymbol{x}_i)\big) = \frac{F_v\big(\phi(\boldsymbol{x}_i)\big) - F_v\big(\phi_h^n(\boldsymbol{x}_i)\big)}{\phi(\boldsymbol{x}_i) - \phi_h^n(\boldsymbol{x}_i)} = f_v\big(\theta_i\phi(\boldsymbol{x}_i) + (1-\theta_i)\phi_h^n(\boldsymbol{x}_i)\big),$$

with $\theta_i \in (0,1), i = 1, 2 \ldots N_h$. Denote $\theta_m = \max_{i=1,\ldots N_h}\theta_i$. One has

$$\theta_m\big(G(\phi), \phi - \phi_h^n\big)_h$$

$$= \sum_{i=1}^{N_h} m_i f_v\big(\theta_i\phi(\boldsymbol{x}_i) + (1-\theta_i)\phi_h^n(\boldsymbol{x}_i)\big)\frac{\theta_m}{\theta_i}\big(\theta_i\phi(\boldsymbol{x}_i) + (1-\theta_i)\phi_h^n(\boldsymbol{x}_i) - \phi_h^n(\boldsymbol{x}_i)\big)$$

$$\geq C\delta_n \sum_{i=1}^{N_h} m_i\Big|f_v\big(\theta_i\phi(\boldsymbol{x}_i) + (1-\theta_i)\phi_h^n(\boldsymbol{x}_i)\big)\Big| - C$$

$$= C\delta_n \sum_{i=1}^{N_h} m_i \left| G\big(\phi(\boldsymbol{x}_i)\big) \right| - C, \tag{3.38}$$

where the second last inequality follows from (3.18). Therefore by taking $\varphi = \theta_m(\phi - \phi_h^n)$ in Eq. (3.7) and utilizing Poincaré's inequality one concludes

$$\delta_n ||I_h(G(\phi))||_{1,h} + \theta_m \delta_n ||I_h(f_v(\phi))||_{1,h} + ||\nabla\phi||^2 \le C||\nabla\mu|| \cdot ||\phi - \phi_h^n||_h + C. \tag{3.39}$$

In light of the uniform boundedness of ϕ and ϕ_h^n, Eq. (3.7) then implies

$$\left| \int_\Omega \mu \, d\boldsymbol{x} \right| \le C(||\nabla\mu|| + 1),$$

hence

$$||\mu||_{H^1} \le C(||\nabla\mu|| + 1). \tag{3.40}$$

Therefore the inequality (3.37) becomes

$$\big(T(\mu), \mu\big) \ge C||\mu||_{H^1}^2 - C,$$

whence the coercivity of T is established.

It follows from the Browder-Minty lemma [37] that there exists a unique solution $\mu \in Y_h$ such that

$$0 = \big(T(\mu), \varphi\big) = (\phi - \phi_h^n, \varphi) - \Delta t([\tilde{\phi}_h^{n+\frac{1}{2}}]\boldsymbol{u}, \nabla\varphi) + \Delta t(\nabla\mu_p, \nabla\varphi), \quad \forall\varphi \in Y_h.$$

Step 4: We establish the energy law, thereby removing the μ dependency of δ in Step 2. We also highlight the solutions on h and n.

We recall from [37] the following classical identity

$$\begin{aligned}\left(\tilde{\phi}_h^{n+\frac{1}{2}}, (\phi_h^{n+1} - \phi_h^n)\right) &= \frac{1}{2}(||\phi_h^{n+1}||^2 - ||\phi_h^n||^2) \\ &- \frac{1}{4}\left\{||\phi_h^{n+1} - \phi_h^n||^2 - ||\phi_h^n - \phi_h^{n-1}||^2 + ||\phi_h^{n+1} - 2\phi_h^n + \phi_h^{n-1}||^2\right\}.\end{aligned} \tag{3.41}$$

Therefore by taking $\varphi = \Delta t \mu_h^{n+\frac{1}{2}}$ in Eq. (3.6), $\varphi = \phi_h^{n+1} - \phi_h^n$ in Eq. (3.7), $\varphi = \Delta t p_h^{n+\frac{1}{2}}$ in Eq. (3.8), respectively, and testing Eqs. (3.9) with $\Delta t \boldsymbol{u}_h^{n+\frac{1}{2}}$, one obtains

$$\begin{aligned}&\int_\Omega I_h F_v(\phi_h^{n+1}) + F_n(\phi_h^{n+1}) + \frac{1}{2}||\nabla\phi_h^{n+1}||^2 \, d\boldsymbol{x} + \frac{1}{4}||\phi_h^{n+1} - \phi_h^n||^2 \\ &+ \Delta t \int_\Omega \eta([\tilde{\phi}_h^{n+\frac{1}{2}}])|\boldsymbol{u}_h^{n+\frac{1}{2}}|^2 + |\nabla\mu^{n+\frac{1}{2}}|^2 \, d\boldsymbol{x} + \Delta t \int_\Omega \rho([\tilde{\phi}_h^{n+\frac{1}{2}}])\mathbf{k} \cdot \boldsymbol{u}_h^{n+\frac{1}{2}} \, d\boldsymbol{x} \\ &\le \int_\Omega I_h F_v(\phi_h^n) + F_n(\phi_h^n) + \frac{1}{2}||\nabla\phi_h^n||^2 \, d\boldsymbol{x} + \frac{1}{4}||\phi_h^n - \phi_h^{n-1}||^2.\end{aligned} \tag{3.42}$$

Taking $\varphi = z$ (3D) in the continuity equation (3.13) yields

$$\Delta t \int_\Omega \rho([\tilde{\phi}_h^{n+\frac{1}{2}}])\mathbf{k} \cdot \boldsymbol{u}_h^{n+\frac{1}{2}} \, d\boldsymbol{x} = \int_\Omega \rho(\phi_h^{n+1})z - \rho(\phi_h^n)z \, d\boldsymbol{x}.$$

The inequality (3.42) now becomes

$$E_d^{n+1} + \Delta t \int_\Omega \eta([\tilde{\phi}_h^{n+\frac{1}{2}}])|\boldsymbol{u}_h^{n+\frac{1}{2}}|^2 + |\nabla\mu_{p,h}^{n+\frac{1}{2}}|^2 \, d\boldsymbol{x} \le E_d^n, \tag{3.43}$$

with

$$E_d^{n+1} = \int_\Omega I_h F_v(\phi_h^{n+1}) + F_n(\phi_h^{n+1}) + \frac{1}{2}||\nabla\phi_h^{n+1}||^2 + \rho(\phi_h^{n+1})z \, d\boldsymbol{x} + \frac{1}{4}||\phi_h^{n+1} - \phi_h^n||^2.$$

The energy law (3.19) follows by taking summation of (3.43) from $n = 1$ to $n = m$ for any $1 \le m \le M - 1$.

To remove the μ dependence in δ_μ (cf. (3.25)), one takes $\varphi = \phi_h^{n+1} - \phi_h^n$ in Eq. (3.7) and utilizes (3.18)

$$\big(F_v(\phi_h^{n+1}), 1\big)_h + ||\nabla\phi_h^{n+1}||^2 + \Delta t\delta_n ||I_h\big(f_v(\phi_h^{n+1})\big)||_{1,h}$$

Table 1
The order of convergence for ϕ and p in L^2 with $h = 8\Delta t$.

$1/h$	$\|e_p\|$	order	$\|e_\phi\|$	order
16	7.2261E-2		6.8854E-3	
32	2.3475E-2	1.62	1.7559E-3	1.97
64	6.9144E-3	1.76	4.412E-4	1.99
128	1.9131E-3	1.85	1.1044E-4	2.00
256	5.0869E-4	1.91	2.7617E-5	2.00

$$+ \Delta t\delta_\mu ||I_h\left(f_v(\phi_h^n)\right)||_{1,h} \le C||\nabla \mu_h^{n+\frac{1}{2}}||^2 + C_s, \tag{3.44}$$

where C_s is the constant on the right-hand side of the energy inequality (3.19). In light of the estimate (3.36), one has

$$||\nabla \mu_h^{n+\frac{1}{2}}|| \le C||\sqrt{\eta}\boldsymbol{u}^{n+\frac{1}{2}}|| + C||\nabla \mu_{p,h}^{n+\frac{1}{2}}|| + C.$$

The energy inequality (3.19) then implies

$$\Delta t||\nabla \mu_h^{n+\frac{1}{2}}|| \le CC_s,$$

hence

$$\Delta t\delta_n ||I^h\left(f_v(\phi_h^{n+1})\right)||_{1,h} \le \frac{CC_s}{\Delta t}. \tag{3.45}$$

Following the same lines of argument as (3.24)–(3.25), one concludes that there exists a small $\delta_{n+1} > 0$ depending on $\phi_0, \eta_1, \eta_2, \rho_1, \rho_2$, the domain Ω, and in particular $h, \Delta t, \delta_n$ such that

$$|\phi_h^{n+1}(\boldsymbol{x}_i)| \le 1 - \delta_{n+1}, \quad i = 1 \dots N_h.$$

This completes the proof. □

Remark 3.1. It is clear from the proof that for fixed h and Δt there exists a $\delta \in (0,1)$ dependent on $\delta_0, \phi_0, \eta_1, \eta_2, \rho_1, \rho_2, \Omega$, h, and Δt such that

$$|\phi_h^n(\boldsymbol{x}_i)| < 1 - \delta, \quad n = 1, 2 \dots M, i = 1 \dots N_h.$$

We comment on that the proposed numerical scheme is unconditional stable as shown in Theorem 3.1, which allows the use of fairly larger time steps while still maintaining the monotonic decay of discrete energy. However, the larger time step size may lead to the loss of numerical accuracy in regions of rapid evolution. Therefore, we choose appropriately small time step size in numerical simulations to guarantee the accuracy of the simulation.

4. Numerical experiments

In this section, we report numerical results to validate the accuracy and efficient of proposed second order finite element numerical scheme for qCHD system with singular logarithmic potential. Newton's iteration method is utilized to solve the nonlinear system. We first provide numerical tests to verify the convergence order and the predicted energy dissipation law. Then, we investigate the scenario of interface pinch off with different densities by buoyancy force to validate the good performance of numerical method. The Saffman-Taylor instability, the rising bubble and the three-dimensional bubble coalescence are numerically simulated to further illustrate that the developed numerical method is resilient in capturing interface. Throughout, we set $\theta = 1$, $\theta_c = 2$.

Example 1 *(Accuracy and convergence).* Set the computational domain is $\Omega = [0,1]^2$. Choosing parameters Π, ϵ, Ca^*, B_0, Pe and χ are one except $\rho_1 = 1$, $\rho_2 = 3$, $\eta_1 = 1$ and $\eta_2 = 3$. The source terms are assumed to be satisfied so that the exact solutions of the qCHD system are as follows

$$p(x,y,t) = \sin(\pi t)\sin(2\pi x),$$
$$\phi(x,y,t) = \frac{1}{\pi}\cos(\pi t)\sin(2\pi x)\cos(2\pi y).$$

We use P_1 finite element for pressure p, phase function ϕ and chemical potential μ. In order to validate the optimal convergence rate of proposed method, we assume that time step size and spatial mesh size satisfied linear relation. By refining mesh size from $h = \frac{1}{16}$ to $h = \frac{1}{256}$, the numerical errors of variables p and ϕ are displayed in Table 1 with $h = 8\Delta t$ at terminate time $T = 1$. From Table 1, it is observed that the numerical errors have the anticipated second order accuracy in L^2 norm for both p and ϕ.

In order to improve the numerical accuracy of diffuse interface problem, adaptive mesh refinement are preferable to resolve the transition layer [43,62], namely, the locally fine mesh is utilized on interface layer, since small sizes of spatial mesh only required

across the thin interface region. In the following numerical experiments, we perform adaptive mesh strategy according to the Hessian of the order parameter. We take the root-level with uniform mesh $h = \frac{1}{64}$, and then explore adaptive mesh refinement.

Example 2 *(Energy dissipation).* In this numerical test, we simulate the coalescence of two drops with different densities and viscosities to validate the preserving of mass and energy dissipation law of the proposed second order numerical method. Two heavier drops is set in a lighter medium. The gravity force is ignored in this experience. The initial position of phase variable is given by

$$\phi = \begin{cases} \tanh\left(\dfrac{r - \sqrt{(x-0.4)^2 + (y-0.4)^2}}{\sqrt{2}\epsilon}\right), & \text{if} \quad x + y < 1 \\ \tanh\left(\dfrac{r - \sqrt{(x-0.6)^2 + (y-0.6)^2}}{\sqrt{2}\epsilon}\right), & \text{otherwise} \end{cases} \tag{4.1}$$

where the radius of dropt is $r = 0.1\sqrt{2}$. Choose parameters $\rho_1 = 1$, $\eta_1 = 1$, $\Pi = 5$, $\epsilon = 0.01$, $Ca^* = 100$, $B_0 = 0$, $Pe = 10$, and $\Delta t = 0.005$. In order to improve the efficiency in capturing the interface, we adopt adaptive mesh strategy with the finer mesh size $\frac{1}{128}$ to perform the simulation on domain $\Omega = [0,1]^2$. We investigate the effect of merging dynamics for cases (a) $\rho_2 = 10$, $\eta_2 = 1$; (b) $\rho_2 = 1$, $\eta_2 = 5$; (c) $\rho_2 = 10$, $\eta_2 = 5$; (d) $\rho_2 = 1$, $\eta_2 = 1$.

Fig. 1 shows the merging dynamics of the kissing drop contour for $\rho_2 = 10, \eta_2 = 1$, $\rho_2 = 1, \eta_2 = 5$ and $\rho_2 = 10, \eta_2 = 5$. We can clearly see that two drops gradually merge into one larger drop. Comparing Figs. 1(a) and 1(c), it is clear that the rate of interface deformation is lower for variable viscosity drops than for matched viscosity, i.e. $\eta_1 = 1$, $\eta_2 = 1$. Since the dynamics of the morphology for variable phase is similar for $\rho_2 = 1, \eta_2 = 1$, we omit the corresponding evolution of the drops for brevity.

Fig. 2 plots the evolution of the discrete energy $E^n - E^0$ and the total volume $\int_\Omega \phi_h^n \, d\boldsymbol{x}$, respectively, showing that the numerical method indeed satisfies the non-increasing energy and the conservation of mass (i.e. the preservation of the drop volume) for both the matched and the variable density and viscosity cases, as predicted in Theorem 3.1. As can be seen from 2(a), the energy decay for the matched case is slower than that for the variable density case, especially when comparing the cases of $\rho_2 = 10$, $\eta_2 = 5$ and $\rho_2 = 1$, $\eta_2 = 5$, due to the lower surface tension in the matched case. This is consistent with the asymptotic analysis in [47] and numerical simulations in [34]. Moreover, for variable viscosities at fixed densities (e.g., $\rho_2 = 10$, $\eta_1 = 5$ and $\rho_2 = 10$, $\eta_1 = 1$), the energy decrease is increased for larger ratio of viscosity, which is consistent with the faster deformation of coalescing drops as shown in Fig. 1. The observed numerical phenomena are in good agreement with the numerical results reported in [34].

Example 3 *(Pinch-off of interface).* We validate the capability in capturing topology transition of interface of the proposed numerical method. We set that a light fluid sandwiched between layers of heavy fluid at initial time. The parameters are $\rho_1 = 1$, $\rho_2 = 5$, $\Pi = 1.2$, $\epsilon = 0.01$, $Ca^* = 100$, $B_0 = 29.46$, $Pe = 10$, the time step size $\Delta t = 0.001$ and the computational domain is a unit square. The initial condition of phase variable is chosen as

$$\phi_0(x,y) = 1 - \frac{1}{2}\xi_+(x,y)\xi_-(x,y), \tag{4.2}$$

with $\xi_\pm(x,y) = 1 \pm \tanh\left(\frac{4}{3\epsilon}\left(y - \frac{1}{3} \pm \frac{1}{4\pi}\left(1 + \frac{\cos(2\pi x)}{2}\right)\right)\right)$, which yields that a blue color is associated to ρ_1 corresponding to a light fluid, a red color is associated to ρ_2 corresponding to a hevy fluid.

Fig. 3 exhibits the contours of phase variable, where the red color and the blue color indicate different phases in heavy and light media, respectively, for both two cases: $\eta_1 = 5$, $\eta_2 = 1$ and $\eta_1 = 1$, $\eta_2 = 5$. It clearly shows the formation and the rising of lighter bubble, include the break up of bridge for no satellite in Figs. 3(a) and one satellite in 3(b). Moreover, in order to further verify the robustness of proposed numerical scheme in capturing interface instability, we take $\eta_1 = 1$ and $\eta_2 = 5$ as well as $\frac{1}{Pe} = 0.1\sqrt{(1-\phi^2)^2 + \epsilon^2}$. The characterized morphology is plotted in Fig. 4. We clearly observe that two satellite drops produce after rupture. The similar numerical finding under Buoyancy-driven flow are obtained in [38,24]. The reasonable phenomenon verify the compatibility of designed numerical schemes.

Example 4 *(Viscous fingering).* We simulate the viscous fingering phenomenon known as Saffmann-Taylor instability to validate the capability of proposed second order numerical method in dealing binary fluids with different viscous.

Choose $\rho_1 = 1$, $\rho_2 = 5$, $\Pi = 1.2$, $\epsilon = 0.01$, $Ca^* = 120$, $\frac{1}{Pe} = \sqrt{(1-\phi^2)^2 + \epsilon^2}$, $\Delta t = 0.0001$, we adopt the double well potential under the absence of gravity on $\Omega = [0, 0.5] \times [0, 1.0]$. The initial condition is chosen as

$$\phi_0(x,y) = \tanh\left(\frac{4}{3\epsilon}\left(y - \frac{1}{10} + \frac{\cos(16\pi x)}{100}\right)\right), \tag{4.3}$$

which yields the set up in Fig. 5(a). A less viscous fluid associated to η_1 is injected into a more viscous fluid associated to η_2 by a velocity $v_{inj} = 50$ at the bottom boundary, the heavy fluid is exacted at the same rate at the top boundary. Fig. 5 displays the insurgency of finger phenomenon with $\eta_1 = 1$ and $\eta_2 = 10$. Fig. 6 compare the deformation and development of finger patter with different viscosity ratios $\eta_2 = 5, 10, 20$, respectively, at characterized time. The expected numerical phenomenon highlight that a large viscous ratio enhances the length of finger morphology that are in coincide with the numerical results reported in [12,38].

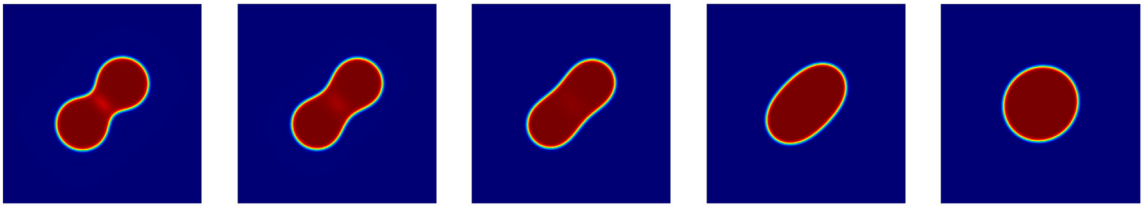

(a) $\rho_2 = 10$, $\eta_2 = 1$ and snapshots are taken at $t = 0.25, 0.5, 1.0, 3.0, 10.0$.

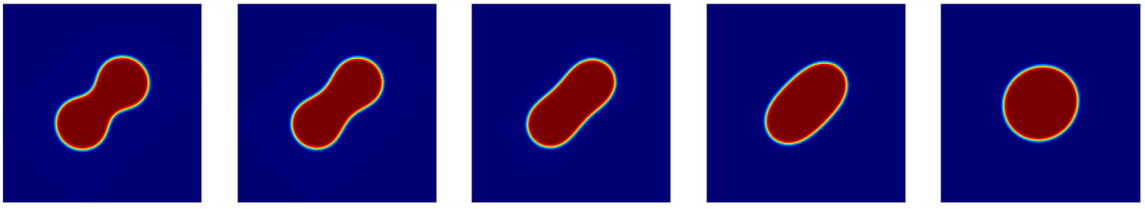

(b) $\rho_2 = 1$, $\eta_2 = 5$ and snapshots are taken at $t = 0.5, 1.0, 2.0, 5.0, 20$.

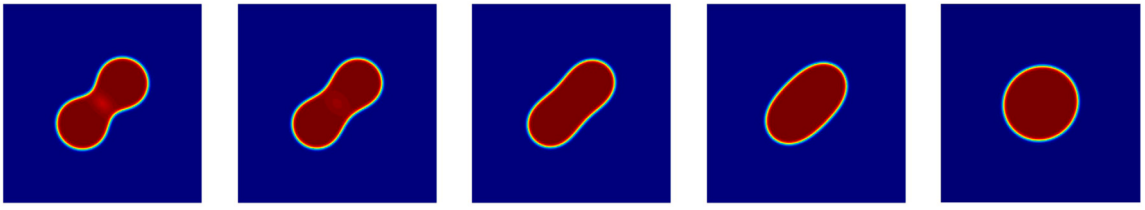

(c) $\rho_2 = 10$, $\eta_2 = 5$ and snapshots are taken at $t = 0.5, 1.0, 2.0, 5.0, 20$.

Fig. 1. The merging evolution of phase variable for two droplets.

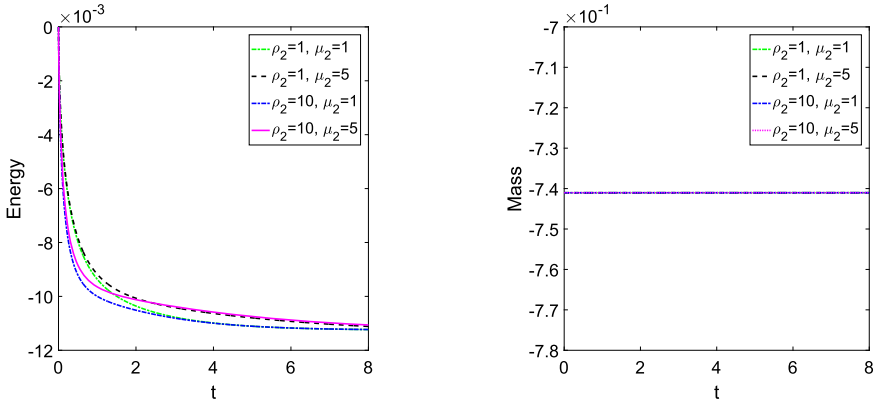

Fig. 2. Evolution of the discrete energy and mass for merging droplets.

Example 5 *(Rising bubble).* In this test, we simulate a light rising bubble in a heavier medium to validate the efficiency of proposed numerical method with respect to different density variations. The computational domain is taken as $\Omega = [0, 1] \times [1, 1.5]$. The initial position of phase function is set as

$$\phi_0(x, y) = \tanh\left(\frac{0.2 - \sqrt{(x-0.5)^2 + (y-0.5)^2}}{\sqrt{2}\epsilon}\right). \tag{4.4}$$

Taking parameters $\eta_1 : \eta_2 = 1 : 2$, $\rho_1 = 1$, $\Pi = 1.2$, $\epsilon = 0.01$, $Ca^* = 120$, $B_0 = 12$, $\frac{1}{Pe} = \sqrt{(1-\phi^2)^2 + \epsilon^2}$, and uniform time step size $\Delta t = 0.0001$, the evolution of bubble is presented in Fig. 7 under the influence of buoyancy with $\rho_2 = 10$ and $\rho_2 = 500$. Compared

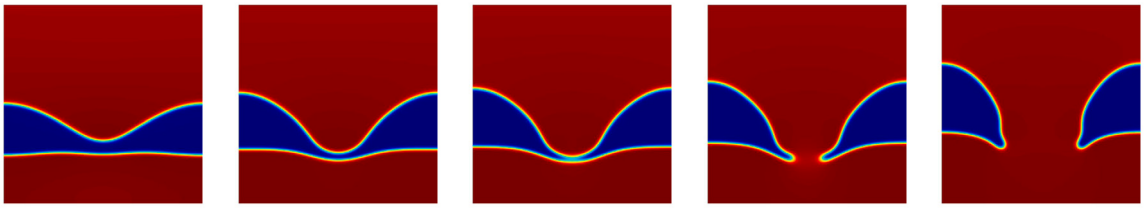

(a) $\eta_1 : \eta_2 = 5 : 1$ and snapshots are taken at $t = 0.1, 0.18, 0.21, 0.25, 0.35$.

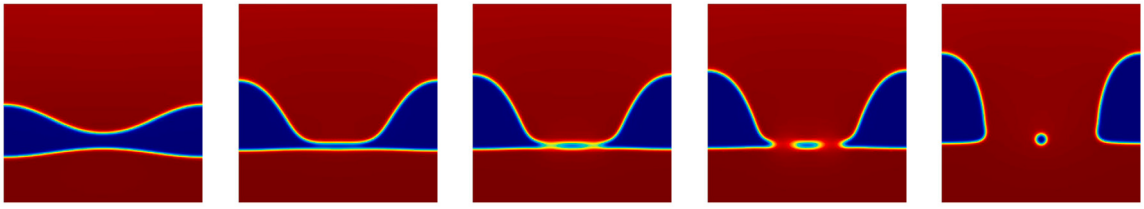

(b) $\eta_1 : \eta_2 = 1 : 5$ and snapshots are taken at $t = 0.1, 0.27, 0.30, 0.32, 0.40$.

Fig. 3. The evolution of phase variable for interface pinchoff. (For interpretation of the colors in the figure(s), the reader is referred to the web version of this article.)

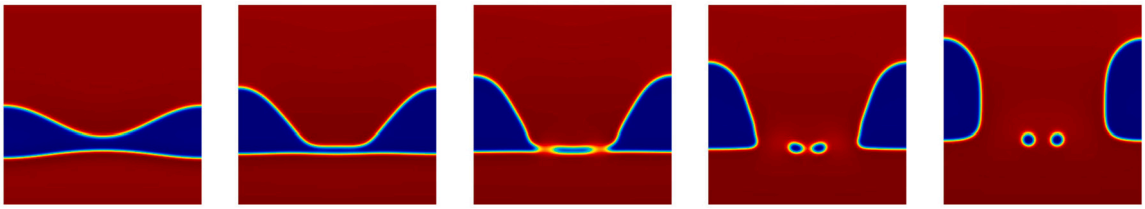

Fig. 4. The evolution of phase variable for interface pinchoff at $t = 0.1, 0.23, 0.29, 0.35, 0.45$.

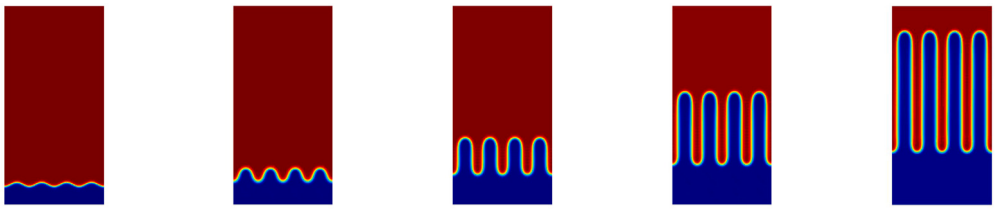

(a) $t = 0.0$ (b) $t = 0.01$ (c) $t = 0.03$ (d) $t = 0.06$ (e) $t = 0.1$

Fig. 5. The evolution of phase variable for viscous fingering under $\eta_2 = 10$

Fig. 7(a) and Fig. 7(b), one can easily observe that the bubble rises with slight deformation in the case $\rho_1 : \rho_2 = 1 : 10$, while the deformation of bubble is more apparent and rises more quickly for a larger density ratio $\rho_1 : \rho_2 = 1 : 500$.

Example 6 *(Three-dimensional merging bubbles).* The interaction and merging for multiple bubbles are inevitable in various engineering applications [2,50,63]. In this experiment, we consider the dynamics of two merging bubbles in three dimensions to validate the capability of proposed numerical method. The initial two spherical bubbles have the same size with a radius of 0.15. The initial position of phase function is placed as shown in the first figure of Figs. 8(a) and 8(b) for the laterally aligned bubbles and the vertically coaxial two bubbles, respectively. Taking $\rho_1 : \rho_2 = 1 : 5$, $\eta_1 : \eta_2 = 1 : 2$, $\Pi = 1.2$, $\epsilon = 0.03$, $Ca^* = 30$, $B_0 = 2.946$, $Pe = 10$, $\Delta t = 0.005$, the computational domain is set as a vertical channel $[0, 0.6] \times [0, 0.9] \times [0, 1.2]$.

Fig. 8 displays the morphotype evolution of zero isosurface. As Fig. 8 indicates, two spherical bubbles contact each other and coalesce under surface tension and moving upwards under buoyancy force. From Fig. 8(a), one can clearly see that the merged bubble slightly expand in the vertical, leading to bubble merging in the lateral configuration. There is the apparent distortion of interface for trailing bubble as shown in Fig. 8(b). As the bubbles rise, the trailing bubble can catch up with the leading bubble

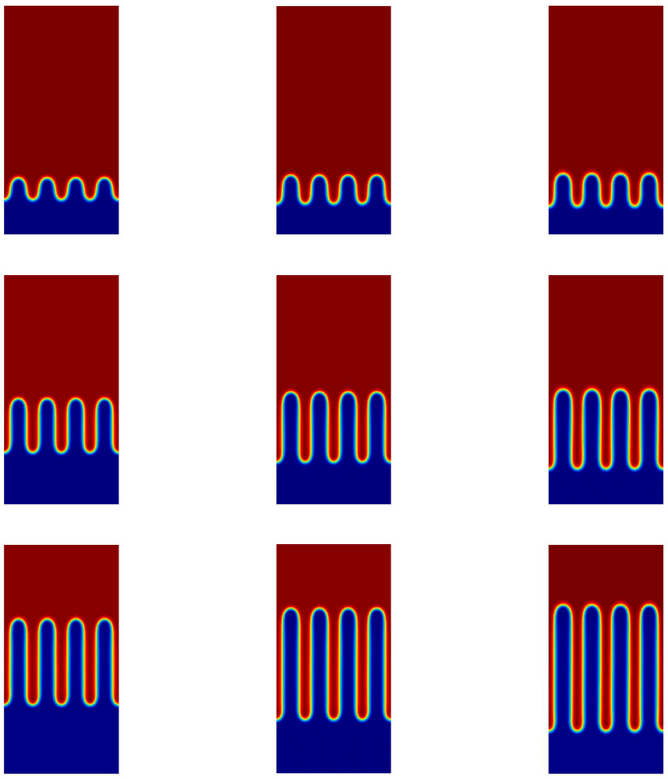

(a) $\eta_2 = 5$ (b) $\eta_2 = 10$ (c) $\eta_2 = 20$

Fig. 6. The evolution of phase variable with different viscosity ratios, and snapshots are taken at $t = 0.02, 0.05, 0.08$.

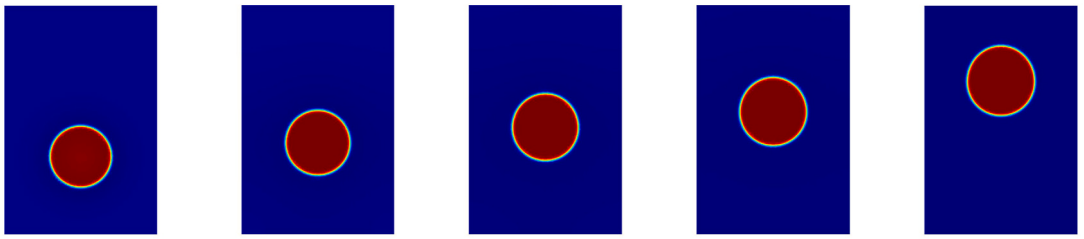

(a) $\rho_2 = 50$, snapshots are taken at $t = 0.01, 0.1, 0.2, 0.3, 0.5$.

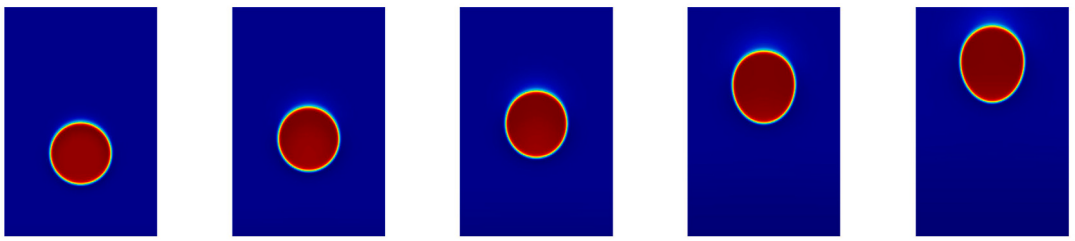

(b) $\rho_2 = 500$, snapshots are taken at $t = 0.001, 0.003, 0.005, 0.01, 0.013$.

Fig. 7. The evolution of phase variable for rising bubble.

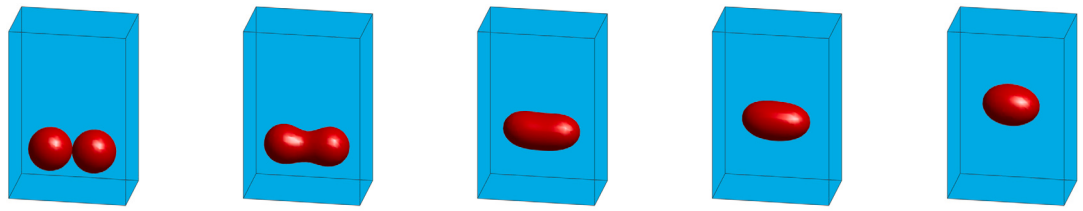

(a) lateral bubbles, snapshots are taken at $t = 0.0, 0.1, 0.4, 0.6, 0.9$.

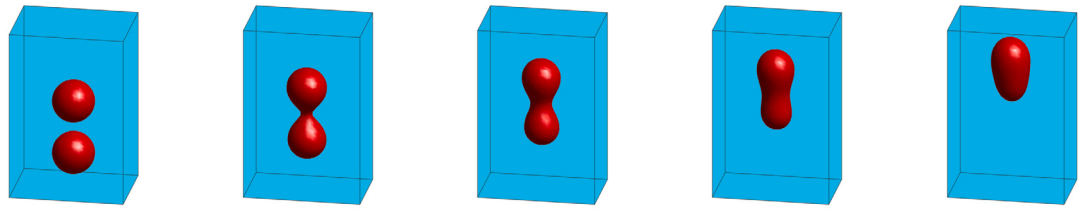

(b) coaxial bubbles, snapshots are taken at $t = 0.0, 0.3, 0.5, 0.7, 1.0$.

Fig. 8. The evolution of bubble coalescence in lateral side-by-side (top) and the vertical coaxial (bottom).

and then the two bubbles mix together to form a big bubble. The reasonable coalescence phenomenon is similar with numerical observations recorded in [3,32].

5. Conclusion

In this paper, we propose a second order finite element method satisfying bound-preserving, mass conservation and energy dissipation for numerically solving the quasi-incompressible Cahn-Hilliard-Darcy system. The key idea is second-order convex-splitting (Crank-Nicolson approximation with Admas-Bashforth extrapolation) for the logarithmic potential. To maintain bound-preservation, the convex part of the singular potential is added back to the equation as a temporal perturbation. This yields a discrete L^1 estimate of the singular potential, thereby preserving the desired bounds for the order parameter. The method is applicable for solving the Cahn-Hilliard-Navier-Stokes equations of matched densities (Model H), and could be generalized for higher order spatial accuracy.

CRediT authorship contribution statement

Yali Gao: Writing – original draft, Visualization, Validation, Methodology, Investigation. **Daozhi Han:** Writing – review & editing, Methodology, Formal analysis, Conceptualization. **Xiaoming Wang:** Writing – review & editing, Methodology, Formal analysis, Conceptualization.

Declaration of competing interest

The authors declare that they have no known competing financial interests or personal relationships that could have appeared to influence the work reported in this paper.

Data availability

Data will be made available on request.

Acknowledgement

The work of Y. Gao is partially supported by the National Natural Science Foundation of China grant 12371406 and 11931013, Young Talent Fund of Xi'an Association for Science and Technology grant 959202413091, Guangdong Basic and Applied Basic Research Foundation, PR China 2023A1515010697. The work of D. Han is supported by the National Science Foundation grant DMS-2310340. The work of X. Wang is supported by the National Natural Science Foundation of China grant 12271237.

References

[1] J.W. Barrett, J.F. Blowey, H. Garcke, Finite element approximation of the Cahn-Hilliard equation with degenerate mobility, SIAM J. Numer. Anal. 37 (1) (1999) 286–318.

[2] G. Brereton, D. Korotney, Coaxial and oblique coalescence of two rising bubbles, in: G. Tryggvason, I. Sahin (Eds.), Dynamics of Bubbles and Vortices Near a Free Surface, vol. 119, ASME, 1991.
[3] C. Chen, X. Yang, Fully-discrete finite element numerical scheme with decoupling structure and energy stability for the Cahn–Hilliard phase-field model of two-phase incompressible flow system with variable density and viscosity, ESAIM: Math. Model. Numer. Anal. 55 (5) (2021) 2323–2347.
[4] J. Chen, S. Sun, X. Wang, Homogenization of two-phase fluid flow in porous media via volume averaging, J. Comput. Appl. Math. 353 (2019) 265–282.
[5] W. Chen, C. Wang, X. Wang, S.M. Wise, Positivity-preserving, energy stable numerical schemes for the Cahn-Hilliard equation with logarithmic potential, J. Comput. Phys. X 3 (2019) 100031.
[6] W. Chen, J. Jing, C. Wang, X. Wang, S.M. Wise, A modified Crank-Nicolson numerical scheme for the Flory-Huggins Cahn-Hilliard model, Commun. Comput. Phys. 31 (1) (2022) 60–93.
[7] Q. Cheng, J. Shen, A new Lagrange multiplier approach for constructing structure preserving schemes, II. Bound preserving, SIAM J. Numer. Anal. 60 (3) (2022) 970–998.
[8] S. Chono, T. Tsuji, J. Sun, Numerical simulation of molding Hele-Shaw flow of polymeric liquid crystals, J. Fluid Sci. Technol. 2 (2) (2007) 368–379.
[9] M.I.M. Copetti, C.M. Elliott, Numerical analysis of the Cahn-Hilliard equation with a logarithmic free energy, Numer. Math. 63 (1) (1992) 39–65.
[10] L. Cueto-Felgueroso, R. Juanes, A phase-field model of two-phase Hele-Shaw flow, J. Fluid Mech. 758 (2014) 522–552.
[11] K.R. Daly, T. Roose, Homogenization of two fluid flow in porous media, Proc. R. Soc. A 471 (2176) (2015) 20140564.
[12] L. Dedè, H. Garcke, K.F. Lam, A Hele-Shaw-Cahn-Hilliard model for incompressible two-phase flows with different densities, J. Math. Fluid Mech. 20 (2) (2018) 531–567.
[13] A.E. Diegel, C. Wang, X. Wang, S.M. Wise, Convergence analysis and error estimates for a second order accurate finite element method for the Cahn-Hilliard-Navier-Stokes system, Numer. Math. 137 (3) (2017) 495–534.
[14] Q. Du, L. Ju, X. Li, Z. Qiao, Maximum bound principles for a class of semilinear parabolic equations and exponential time-differencing schemes, SIAM Rev. 63 (2) (2021) 317–359.
[15] C.M. Elliott, A.M. Stuart, The global dynamics of discrete semilinear parabolic equations, SIAM J. Numer. Anal. 30 (6) (1993) 1622–1663.
[16] D.J. Eyre, Unconditionally gradient stable time marching the Cahn-Hilliard equation, MRS Online Proc. Libr. Arch. 529 (1998) 39–46.
[17] R. Farajzadeh, A. Andrianov, P.L.J. Zitha, Investigation of immiscible and miscible foam for enhancing oil recovery, Ind. Eng. Chem. Res. 49 (4) (2010) 1910–1919.
[18] X. Feng, S.M. Wise, Analysis of a Darcy-Cahn-Hilliard diffuse interface model for the Hele-Shaw flow and its fully discrete finite element approximation, SIAM J. Numer. Anal. 50 (3) (2012) 1320–1343.
[19] F. Frank, A. Rupp, D. Kuzmin, Bound-preserving flux limiting schemes for DG discretizations of conservation laws with applications to the Cahn-Hilliard equation, Comput. Methods Appl. Mech. Eng. 359 (2020) 112665.
[20] G. Fu, A divergence-free HDG scheme for the Cahn-Hilliard phase-field model for two-phase incompressible flow, J. Comput. Phys. 419 (2020) 109671.
[21] G. Fu, S. Osher, W. Li, High order spatial discretization for variational time implicit schemes: Wasserstein gradient flows and reaction-diffusion systems, J. Comput. Phys. 491 (2023) 112375.
[22] F. Gancedo, A survey for the Muskat problem and a new estimate, SeMA J. 74 (1) (2017) 21–35.
[23] V. Ganesan, H. Brenner, A diffuse interface model of two-phase flow in porous media, R. Soc. Lond. Proc., Ser. A, Math. Phys. Eng. Sci. 456 (1996) (2000) 731–803.
[24] Y. Gao, R. Li, L. Mei, Y. Lin, Second-order order decoupled energy stable numerical scheme for Cahn-Hilliard-Hele-Shaw system, Appl. Numer. Math. 157 (2020) 338–355.
[25] K. Glasner, S. Orizaga, Improving the accuracy of convexity splitting methods for gradient flow equations, J. Comput. Phys. 315 (2016) 52–64.
[26] K. Glasner, A diffuse interface approach to Hele-Shaw flow, Nonlinearity 16 (2003) 49–66.
[27] Y. Gong, J. Zhao, Q. Wang, Arbitrarily high-order linear energy stable schemes for gradient flow models, J. Comput. Phys. 419 (2020) 109610.
[28] Y. Gong, J. Zhao, X. Yang, Q. Wang, Fully discrete second-order linear schemes for hydrodynamic phase field models of binary viscous fluid flows with variable densities, SIAM J. Sci. Comput. 40 (1) (2018) B138–B167.
[29] Y. Gong, J. Zhao, Q. Wang, An energy stable algorithm for a quasi-incompressible hydrodynamic phase-field model of viscous fluid mixtures with variable densities and viscosities, Comput. Phys. Commun. 219 (2017) 20–34.
[30] R. Granero-Belinchón, O. Lazar, Growth in the Muskat problem, Math. Model. Nat. Phenom. 15 (7) (2020).
[31] F. Guillén-González, G. Tierra, On linear schemes for a Cahn-Hilliard diffuse interface model, J. Comput. Phys. 234 (2013) 140–171.
[32] Z. Guo, Q. Cheng, P. Lin, C. Liu, J. Lowengrub, Second order approximation for a quasi-incompressible Navier-Stokes Cahn-Hilliard system of two-phase flows with variable density, J. Comput. Phys. 448 (2022) 110727.
[33] Z. Guo, P. Lin, J. Lowengrub, S.M. Wise, Mass conservative and energy stable finite difference methods for the quasi-incompressible Navier-Stokes-Cahn-Hilliard system: primitive variable and projection-type schemes, Comput. Methods Appl. Mech. Eng. 326 (2017) 144–174.
[34] Z. Guo, P. Lin, J.S. Lowengrub, A numerical method for the quasi-incompressible Cahn-Hilliard-Navier-Stokes equations for variable density flows with a discrete energy law, J. Comput. Phys. 276 (2014) 486–507.
[35] D. Han, A decoupled unconditionally stable numerical scheme for the Cahn-Hilliard-Hele-Shaw system, J. Sci. Comput. 66 (3) (2016) 1102–1121.
[36] D. Han, D. Sun, X. Wang, Two-phase flows in Karstic geometry, Math. Methods Appl. Sci. 37 (18) (2014) 3048–3063.
[37] D. Han, X. Wang, A second order in time, uniquely solvable, unconditionally stable numerical scheme for Cahn-Hilliard-Navier-Stokes equation, J. Comput. Phys. 290 (2015) 139–156.
[38] D. Han, X. Wang, A second order in time, decoupled, unconditionally stable numerical scheme for the Cahn-Hilliard-Darcy system, J. Sci. Comput. 77 (2) (2018) 1210–1233.
[39] Q. He, R. Glowinski, X.-P. Wang, A least-squares/finite element method for the numerical solution of the Navier-Stokes-Cahn-Hilliard system modeling the motion of the contact line, J. Comput. Phys. 230 (12) (2011) 4991–5009.
[40] G.M. Homsy, Viscous fingering in porous media, Annu. Rev. Fluid Mech. 19 (1987) 277–311.
[41] F. Huang, J. Shen, K. Wu, Bound/positivity preserving and unconditionally stable schemes for a class of fourth order nonlinear equations, J. Comput. Phys. 460 (2022) 111177.
[42] D.P. Jackson, J.A. Miranda, Controlling fingering instabilities in rotating ferrofluids, Phys. Rev. E 67 (2003) 017301.
[43] J. Kim, K. Kang, J. Lowengrub, Conservative multigrid methods for Cahn-Hilliard fluids, J. Comput. Phys. 193 (2) (2004) 511–543.
[44] H.G. Lee, J. Lowengrub, J. Goodman, Modeling pinchoff and reconnection in a Hele-Shaw cell. I. The models and their calibration, Phys. Fluids 14 (2) (2002) 492–513.
[45] C. Liu, D. Ray, C. Thiele, L. Lin, B. Riviere, A pressure-correction and bound-preserving discretization of the phase-field method for variable density two-phase flows, J. Comput. Phys. 449 (2022) 110769.
[46] C. Liu, B. Riviere, J. Shen, X. Zhang, A simple and efficient convex optimization based bound-preserving high order accurate limiter for Cahn–Hilliard–Navier–Stokes system, SIAM J. Sci. Comput. 46 (3) (2024) A1923–A1948.
[47] J. Lowengrub, L. Truskinovsky, Quasi-incompressible Cahn-Hilliard fluids and topological transitions, R. Soc. Lond. Proc., Ser. A, Math. Phys. Eng. Sci. 454 (1978) (1998) 2617–2654.
[48] H.W. Lu, K. Glasner, A.l. Bertozzi, C.-J. Kim, A diffuse-interface model for electrowetting drops in a Hele-Shaw cell, J. Fluid Mech. 590 (2007) 411–435.
[49] A. Miranville, The Cahn–Hilliard Equation: Recent Advances and Applications, Society for Industrial and Applied Mathematics, Philadelphia, PA, 2019.

[50] C. Mulbah, C. Kang, N. Mao, W. Zhang, A.R. Shaikh, S. Teng, A review of VOF methods for simulating bubble dynamics, Prog. Nucl. Energy 154 (2022) 104478.
[51] M. Muskat, Two fluid systems in porous media. The encroachment of water into an oil sand, Physics 5 (9) (1934) 250–264.
[52] F. Otto, Evolution of microstructure in unstable porous media flow: a relaxational approach, Commun. Pure Appl. Math. 52 (7) (1999) 873–915.
[53] P.G. Saffmann, G.I. Taylor, The penetration of a fluid into a porous medium or Hele-Shaw cell containing a more viscous liquid, Proc. R. Soc. Lond. Ser. A 245 (1242) (1958) 312–329.
[54] M. Schmuck, M. Pradas, G.A. Pavliotis, S. Kalliadasis, Upscaled phase-field models for interfacial dynamics in strongly heterogeneous domains, Proc. R. Soc. Lond., Ser. A, Math. Phys. Eng. Sci. 468 (2147) (2012) 3705–3724.
[55] M. Schmuck, M. Pradas, G.A. Pavliotis, S. Kalliadasis, Derivation of effective macroscopic Stokes-Cahn-Hilliard equations for periodic immiscible flows in porous media, Nonlinearity 26 (12) (2013) 3259–3277.
[56] J. Shen, C. Wang, X. Wang, S.M. Wise, Second-order convex splitting schemes for gradient flows with Ehrlich-Schwoebel type energy: application to thin film epitaxy, SIAM J. Numer. Anal. 50 (1) (2012) 105–125.
[57] J. Shen, J. Xu, J. Yang, The scalar auxiliary variable (SAV) approach for gradient flows, J. Comput. Phys. 353 (2018) 407–416.
[58] J. Shen, J. Xu, J. Yang, A new class of efficient and robust energy stable schemes for gradient flows, SIAM Rev. 61 (3) (2019) 474–506.
[59] J. Shen, X. Yang, Numerical approximations of Allen-Cahn and Cahn-Hilliard equations, Discrete Contin. Dyn. Syst. 28 (4) (2010) 1669–1691.
[60] J. Shen, X. Yang, Decoupled, energy stable schemes for phase-field models of two-phase incompressible flows, SIAM J. Numer. Anal. 53 (1) (2015) 279–296.
[61] L. Shen, H. Huang, P. Lin, Z. Song, S. Xu, An energy stable C^0 finite element scheme for a quasi-incompressible phase-field model of moving contact line with variable density, J. Comput. Phys. 405 (2020) 109179.
[62] M. Sussman, A.S. Almgren, J.B. Bell, P. Colella, L.H. Howell, An adaptive level set approach for incompressible two-phase flows, J. Comput. Phys. 148 (1999) 81–124.
[63] M. van Sint Annaland, N.G. Deen, J.A.M. Kuipers, Numerical simulation of gas bubbles behaviour using a three-dimensional volume of fluid method, Chem. Eng. Sci. 60 (11) (2005) 2999–3011.
[64] S.M. Wise, J. Lowengrub, H. Frieboes, V. Cristini, Three-dimensional multispecies nonlinear tumor growth-I model and numerical method, J. Theor. Biol. 253 (3) (2008) 524–543.
[65] X. Yang, J. Zhao, Q. Wang, Numerical approximations for the molecular beam epitaxial growth model based on the invariant energy quadratization method, J. Comput. Phys. 333 (2017) 104–127.
[66] X. Yang, L. Ju, Linear and unconditionally energy stable schemes for the binary fluid-surfactant phase field model, Comput. Methods Appl. Mech. Eng. 318 (2017) 1005–1029.
[67] M. Yuan, W. Chen, C. Wang, S.M. Wise, Z. Zhang, A second order accurate in time, energy stable finite element scheme for the Flory-Huggins-Cahn-Hilliard equation, Adv. Appl. Math. Mech. 14 (6) (2022) 1477–1508.
[68] X. Zhang, C.-W. Shu, On maximum-principle-satisfying high order schemes for scalar conservation laws, J. Comput. Phys. 229 (9) (2010) 3091–3120.
[69] M. Zhang, T. Maxworthy, The interactive dynamics of flow and directional solidification in a Hele-Shaw cell Part I. Experimental investigation of parallel shear flow, J. Fluid Mech. 470 (2002) 247–268.
[70] J. Zhao, X. Yang, Y. Gong, Q. Wang, A novel linear second order unconditionally energy stable scheme for a hydrodynamic $\mathbf{Q}$-tensor model of liquid crystals, Comput. Methods Appl. Mech. Eng. 318 (2017) 803–825.
[71] L. Zhornitskaya, A.L. Bertozzi, Positivity-preserving numerical schemes for lubrication-type equations, SIAM J. Numer. Anal. 37 (2) (2000) 523–555.